Continuous Data Assimilation Enhanced Nonlinear Solvers for the p-Laplace Equation

Lin Mu

Department of Mathematics, University of Georgia, Athens, GA 30602, US
linmu@uga.edu

Abstract. Solving the p-Laplace equation numerically is challenging due to inherent degeneracies and singularities. We present a new hybrid strategy combining Continuous Data Assimilation, Picard iteration with Anderson Acceleration, and Newton's Method. By incorporating coarse-mesh observations via a nudging term, the scheme provides essential spatial regularization. Our results show that this integration stabilizes nonlinear iterations and significantly improves convergence speed. Notably, the CDA-enhanced solver captures localized singular behaviors and suppresses oscillations in highly nonlinear regimes where standard methods typically fail.

Keywords: p-Laplace equation · Finite element methods · Continuous data assimilation · Nonlinear iteration.

1 Introduction

The p-Laplace equation is a fundamental nonlinear partial differential equation (PDE) with wide-ranging applications, including population modeling, image processing, sand pile analysis, and biomolecular solvation energy calculations. The equation is described as: Given $f \in (W^{1,p}(\Omega))^*, u_D \in W^{1,p}(\Omega)$, seek $u \in W^{1,p}(\Omega)$ with

$$-\nabla \cdot (|\nabla u|^{p-2}\nabla u) = f, \text{ in } \Omega, \tag{1}$$

$$u = u_D, \text{ on } \partial\Omega. \tag{2}$$

Here, $p \in (1, \infty)$ is a given parameter, $\Omega \in \mathbb{R}^d (d = 2, 3)$ is a domain with a Lipschitz boundary $\partial\Omega$, and $\nabla\cdot$ and ∇ denote the divergence and gradient operators.

Previous research has primarily focused on solving the variational formulation of the p-Laplacian. For example, [15] combined an effective finite element method (FEM) with Newton's method to provide a robust framework for 2D nonlinearities. Other significant contributions to FEM discretization strategies

ICCS Camera Ready Version 2026
To cite this paper please use the final published version:
DOI: 10.1007/978-3-032-29918-5_11

across diverse regimes include [2, 5, 8, 10–12, 15, 16]. Continuous Data Assimilation (CDA), often implemented via the Azouani-Olson-Titi (AOT) algorithm [1], synchronizes numerical models with real-time observed data by adding a "nudging term" that penalizes deviations from physical observations. While traditionally applied to time-dependent problems [4, 7, 13], CDA was recently proposed in [9] to improve the efficiency and robustness of steady-state nonlinear solvers, a framework later extended by [14] to handle noisy observations in Navier-Stokes equations. In this work, we propose a hybrid strategy that integrates CDA with Anderson Acceleration (AA) and Newton's Method to stabilize nonlinear iterations and accelerate convergence across both singular and degenerate regimes for p-Laplace equations.

The paper is organized as follows: Section 2 introduces the mathematical preliminaries, including the weak formulation and a review of Picard, AA, Newton, and CDA methods. Section 3 proposes a CDA-enhanced numerical schemes and their discretization. In Section4, we detail the integration of Anderson Acceleration with Newton's Method to achieve quadratic convergence, followed by comprehensive numerical experiments across singular and degenerate regimes. Finally, Section 5 provides concluding remarks and summarizes our findings.

2 Preliminaries

We employ standard notations for Sobolev spaces. Let $W^{1,q}(\Omega)$ and $W_0^{1,q}(\Omega)$ be defined as:

$$W^{1,q}(\Omega) = \left\{ v; \int_\Omega |\nabla v|^q < \infty \right\}, \quad W_0^{1,q}(\Omega) = \{ v \in W^{1,q}(\Omega); v|_{\partial\Omega} = 0 \},$$

equipped with the norm $\|\nabla u\|_q = \left(\int_\Omega |\nabla u|^q d\mathbf{x}\right)^{1/q}$. The weak formulation of the problem reads: Seek a weak solution $u \in W^{1,p}(\Omega)$ with $u = u_D$ on $\partial\Omega$ through the variational form:

$$\int_\Omega |\nabla u|^{p-2} \nabla u \cdot \nabla v d\mathbf{x} = \int_\Omega f v d\mathbf{x}, \ \forall v \in W_0^{1,p}(\Omega) \tag{3}$$

Based on continuous embedding theory, the uniqueness of the solution in $W^{1,p}(\Omega)$ ensures it also holds in $H^1(\Omega)$. As a Hilbert space, $H^1(\Omega)$ is more computationally convenient and will be utilized for the nonlinear iterations and numerical experiments in the following sections.

2.1 A Picard algorithm for the p-Laplace equation

The **Picard iteration** for (3) seeks $u^{(k+1)} \in H^1(\Omega)$ with $u^{(k+1)}|_{\partial\Omega} = u_D$ such that for all $v \in H_0^1(\Omega)$:

$$\int_\Omega |\nabla u^{(k)}|^{p-2} \nabla u^{(k+1)} \cdot \nabla v \, d\mathbf{x} = \int_\Omega f v d\mathbf{x}. \tag{4}$$

ICCS Camera Ready Version 2026
To cite this paper please use the final published version:
DOI: 10.1007/978-3-032-29918-5_11

The Picard iteration defined in (4) is a popular choice due to its simplicity and robust global convergence properties. However, its performance is highly sensitive to the value of p. In the degenerate case ($p > 2$), the iteration often exhibits a very slow, sub-linear convergence rate as the solution gradients approach zero. Conversely, in the singular regime ($1 < p < 2$), the method can suffer from instabilities unless an appropriate small relaxation parameters are employed. To accelerate the fixed-point convergence we integrate extrapolation techniques—specifically Anderson Acceleration (AA)—which utilizes iteration history to construct optimal search directions.

The AA algorithm utilizes a history of m previous iterations to determine an optimal combination that minimizes the residual. Let $g(u)$ be the fixed-point map such that $u^{(k+1)} = g(u^{(k)})$, and let $\mathsf{f}_k = g(u^{(k)}) - u^{(k)}$ denote the residual at step k. Given a relaxation parameter $\beta \in (0, 1]$ and history depth $m \geq 1$, the accelerated iterate $u^{(k+1)}$ is computed as:

1. Initialize: $u^{(1)} = g(u^{(0)})$.
2. Iterate: For $k = 1, 2, \ldots$:
   - Set $m_k = \min(k, m)$.
   - Solve for weights $\alpha^{(k)} = (\alpha_0^{(k)}, \ldots, \alpha_{m_k}^{(k)})$ that minimize the multi-secant residual:
   $$\min \left\| \sum_{i=0}^{m_k} \alpha_i^{(k)} \mathsf{f}_{k-m_k+i} \right\|, \quad \text{subject to } \sum_{i=0}^{m_k} \alpha_i^{(k)} = 1. \tag{5}$$
   - Update the solution:
   $$u^{(k+1)} = (1-\beta) \sum_{i=0}^{m_k} \alpha_i^{(k)} u^{(k-m_k+i)} + \beta \sum_{i=0}^{m_k} \alpha_i^{(k)} g(u^{(k-m_k+i)}). \tag{6}$$

While AA significantly enhances performance, it typically yields linear or superlinear convergence. In practice, the performance of AA can be improved by tuning several parameters including relaxation (β), Anderson depth (m), and filtering. More details regarding the effective implementation and tuning can be found in [3, 6]. In this work, we set $\beta = 1$.

2.2 A Newton algorithm for the p-Laplace equation

To achieve faster, quadratic convergence, especially when the initial guess is near the exact solution, Newton's method can be employed. For the p-Laplace equation, the **Newton iteration** $u^{(k+1)} = u^{(k)} + \delta u$ is defined by solving for the update δu in: Find $\delta u \in H_0^1(\Omega)$

$$\begin{aligned} &\int_\Omega \left[(p-2)|\nabla u^{(k)}|^{p-4} (\nabla u^{(k)} \cdot \nabla \delta u) \nabla u_k + |\nabla u^{(k)}|^{p-2} \nabla \delta u \right] \cdot \nabla v \, d\mathbf{x} \\ &= -\int_\Omega |\nabla u^{(k)}|^{p-2} \nabla u_k \cdot \nabla v \, d\mathbf{x} + \int_\Omega f v \, d\mathbf{x}, \quad \forall \delta u \in H_0^1(\Omega). \end{aligned} \tag{7}$$

ICCS Camera Ready Version 2026
To cite this paper please use the final published version:
DOI: 10.1007/978-3-032-29918-5_11

However, Newton's method typically requires a starting guess within its local "convergence ball." We therefore employ a hybrid strategy where AA is utilized as a robust pre-solver to drive the residual below a switching threshold, after which Newton's method is activated to achieve quadratic convergence.

2.3 Continuous Data Assimilation

To further enhance the nonlinear solver, we propose to incorporate a Continuous Data Assimilation (CDA) framework, also known as the AOT algorithm [1]. This approach introduces a nudging term into the iteration, which utilizes coarse-mesh observations to guide the numerical solution. The CDA-enhanced Picard/Newton algorithm is defined as:

$$A(u_k; u_{k+1}) + \mu I_H(u_{k+1} - u_{obs}) = f \tag{8}$$

where $\mu > 0$ is the nudging parameter, I_H is an interpolation operator onto the coarse mesh, and u_{obs} represents the observed data on the coarse mesh. Here A denotes the operator for either Picard or Newton iterations. In the context of the p-Laplacian, this term acts as a spatial regularizer. By penalizing large deviations from the coarse-scale features of the solution, CDA suppresses the non-physical oscillations and instabilities that arise in the degenerate ($p > 2$) and singular ($p < 2$) regimes, ensuring more monotonic convergence.

3 Proposed Numerical Scheme

3.1 Finite Element Scheme

To obtain a numerical solution, we employ the finite element method (FEM) on a uniformly regular triangulation $\{\mathcal{T}_h\}$ of $\bar{\Omega}$ with mesh size bounded by h. We define the continuous piecewise linear finite element spaces as:

$$V_h = \{v_h \in H^1(\Omega) : v_h|_T \in P_1(T), \forall T \in V_h\}, \tag{9}$$

$$V_h^0 = \{v_h \in H_0^1(\Omega) : v_h|_T \in P_1(T), \forall T \in V_h\}. \tag{10}$$

The discrete problem is solved using the following schemes:

Picard FEM scheme: Find $u_h^{(k+1)} \in V_h$ with $u_h^{(k+1)}|_{\partial\Omega} = u_D$ such that for all $v \in V_h^0$:

$$\int_\Omega |\nabla u_h^{(k)}|^{p-2} \nabla u_h^{(k+1)} \cdot \nabla v \, d\mathbf{x} = \int_\Omega f v d\mathbf{x}. \tag{11}$$

CDA-Picard-FEM scheme: Incorporating coarse-mesh observations u_{obs} via an interpolation operator I_H, find $u_h^{(k+1)} \in V_h$ with $u_h^{(k+1)}|_{\partial\Omega} = u_D$ such that for all $v \in V_h^0$:

$$\int_\Omega \left(|\nabla u_h^k|^{p-2} \nabla u_h^{(k+1)} \cdot \nabla v + \mu I_H(u_h^{(k+1)} - u_{\text{obs}}) \right) d\mathbf{x} = \int_\Omega f v d\mathbf{x}. \tag{12}$$

ICCS Camera Ready Version 2026
To cite this paper please use the final published version:
DOI: 10.1007/978-3-032-29918-5_11

Newton FEM scheme: find $u_h^{(k+1)} \in V_h$ and $u_h^{(k+1)}|_{\partial\Omega} = u_D$ such that $\forall v \in V_h^0$,

$$\begin{aligned}&\int_\Omega \left[(p-2)|\nabla u_h^{(k)}|^{p-4}(\nabla u_h^{(k)} \cdot \nabla u_h^{(k+1)})\nabla u_h^{(k)} + |\nabla u_h^{(k)}|^{p-2}\nabla u_h^{(k+1)}\right] \cdot \nabla v \, d\mathbf{x} \\ &= \int_\Omega \left[(p-2)|\nabla u_h^{(k)}|^{p-4}(\nabla u_h^{(k)} \cdot \nabla u_h^{(k)})\nabla u_h^{(k)}\right] \cdot \nabla v + \int_\Omega f v \, d\mathbf{x}. \end{aligned} \tag{13}$$

CDA-Newton FEM scheme: find $u_h^{(k+1)} \in V_h$ and $u_h^{(k+1)}| = u_D$ such that $\forall v \in V_h^0$

$$\begin{aligned}&\int_\Omega \left[(p-2)|\nabla u_h^{(k)}|^{p-4}(\nabla u_h^{(k)} \cdot \nabla u_h^{(k+1)})\nabla u_h^{(k)} + |\nabla u_h^{(k)}|^{p-2}\nabla u_h^{(k+1)}\right] \cdot \nabla v \, d\mathbf{x} \\ &+\mu \int_\Omega I_H(u_h^{(k+1)} - u_{\text{obs}}) d\mathbf{x} \\ &= \int_\Omega \left[(p-2)|\nabla u_h^{(k)}|^{p-4}(\nabla u_h^{(k)} \cdot \nabla u_h^{(k)})\nabla u_h^{(k)}\right] \cdot \nabla v + \int_\Omega f v \, d\mathbf{x}. \end{aligned} \tag{14}$$

In the practical implementation, we sometimes need to add regularization term and modify $|\nabla u_h^{(k)}|$ to $|\epsilon + \nabla u_h^{(k)}|$ (for example ϵ =1E-10). The methods described above-Continuous Data Assimilation, Anderson acceleration, and Newton's method can be integrated into a hierarchical hybrid framework to maximize computational efficiency.

4 Numerical Example

4.1 Example 4.1 - Smooth solution

Let $\Omega = [0,1]^2$ and analytical solution be

$$u = \frac{p-1}{p-s}\left(\frac{1}{2-s}\right)^{1/(p-1)}(1 - r^{\frac{p-s}{p-1}}),\ r = \sqrt{(x+1)^2 + (y+1)^2}, \tag{15}$$

where p and s are two parameters.

Case 1.1. Iteration Counts (Picard Iteration) First, we set $s = 0$ and vary the values in p to test the required iteration counts for achieving $tol < 1e{-}6$. The results illustrated in Fig. 1 (left) provide insights into the performance of the Picard iteration across varying mesh sizes (h) and the nonlinearity parameter p:

- The iteration counts exhibit a distinctive "V-shape" centered around $p = 2$. When $p = 2$, the equation becomes linear, and the Picard iteration converges almost instantly (in a single step). As p deviates from 2—moving toward either the sub-diffusive ($p < 2$) or super-diffusive ($p > 2$) regimes—the number of iterations required to reach the tolerance of 10^{-6} increases significantly.

ICCS Camera Ready Version 2026
To cite this paper please use the final published version:
DOI: 10.1007/978-3-032-29918-5_11

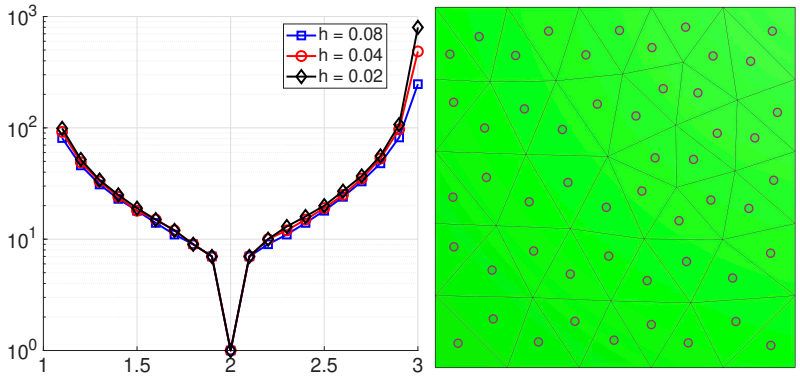

Fig. 1. Example 4.1: Iteration counts of the Picard method as a function of p for varying mesh sizes h, and $s = 0$ (left); Coarse mesh observations with $H = 0.2$ used for the CDA nudging term (right).

- Notably, the iteration counts for $h = 0.08, 0.04$, and 0.02 are nearly identical and overlap across the entire range of p. This suggests that the standard Picard method for this specific problem is relatively robust with respect to spatial refinement, though it remains highly sensitive to the degree of nonlinearity.
- For extreme values (e.g., $p = 1.1$ or $p = 3$), the iteration count exceeds 10^2, highlighting the potential need for the CDA-enhancement to maintain efficiency in more challenging physical regimes.

Case 1.2. Iteration Counts (Picard vs CDA-Picard Iteration) Fig. 2 (left) compares the performance of the standard Picard iteration against the CDA-enhanced version across various values of the nonlinearity parameter p and $h = 0.02$. The CDA observations are piecewise constants sampled at the barycenters of a coarse mesh with size $H = 0.2$ (as shown in Fig. 1 (right)).

- Across the entire range of p, the CDA-enhanced Picard iteration (with $\mu = 100$) consistently requires fewer iterations to reach the target tolerance than the standard Picard method. This demonstrates that incorporating even relatively coarse spatial observations ($H = 0.2$) significantly accelerates the fixed-point convergence.
- Figure 2 (right) illustrates the L^2 error profiles for both the standard Picard and CDA-enhanced Picard iterations of the nonlinearity parameter p, using a fixed mesh size $h = 0.02$ and $s = 0$. Across the entire tested range of $p \in [1.1, 3]$, the CDA-enhanced method (with $\mu = 100$) consistently yields a lower L^2 error compared to the standard Picard iteration. Notably, the error for both methods is highest in the singular regime ($p \to 1$) and gradually decreases as the problem becomes more degenerate ($p \to 3$). The CDA-

ICCS Camera Ready Version 2026
To cite this paper please use the final published version:
DOI: 10.1007/978-3-032-29918-5_11

enhanced version maintains a significantly lower error floor across all values of p, with the performance gap becoming most pronounced in the singular regime. This demonstrates that the CDA not only accelerates convergence but also substantially improves the precision of the numerical solution by providing effective spatial regularization across varying nonlinearity.

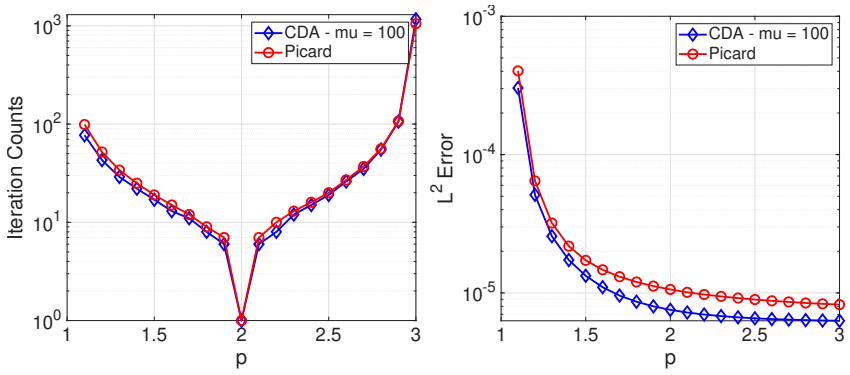

Fig. 2. Example 4.1: Comparison of iteration counts (left) and L^2 error (right) between standard Picard and CDA-enhanced Picard methods for varying p.

Case 1.3 - Accuracy (Picard vs CDA-Picard Iteration) In this test, we choose $p = 1.1$ and $s = 0.97$ to compare the performance of different nudging parameters μ. Again the observations are taken as the data on the grid with $H = 0.2$. Fig. 3 demonstrates the impact of the nudging parameter μ on both the convergence history (left) and the spatial accuracy (right) of the CDA-enhanced Picard iteration.

- Shown in Fig. 3(left): As μ increases from 10 to 1000 for $h = 0.01$, the iteration count required to reach the target tolerance decreases significantly. While the standard Picard method requires approximately 60 iterations to reach an error of 8.96×10^{-6}, the CDA-enhanced version with $\mu = 100$ reaches a much lower error of 1.77×10^{-6} in the same number of steps. It is noted that higher values of μ (e.g., $\mu = 1000$) provide the fastest initial descent in error.
- Shown in Fig. 3(right): Across all tested mesh sizes ($1/h$), the CDA-enhanced methods consistently maintain lower L^2 error levels than the standard Picard iteration. Both the standard Picard and CDA-enhanced methods maintain second-order spatial accuracy. This confirms that the CDA term acts as an effective stabilizer and accelerator without degrading the underlying accuracy of the finite element discretization. while the CDA-enhanced methods

ICCS Camera Ready Version 2026
To cite this paper please use the final published version:
DOI: 10.1007/978-3-032-29918-5_11

consistently outperform the standard Picard iteration, the reduction in L^2 error does not scale infinitely with the nudging parameter μ. In certain mesh regimes, a larger μ (e.g., $\mu = 1000$) may yield slightly higher error compared to moderate values like $\mu = 100$. This suggests that simply increasing μ is not always optimal for achieving the lowest possible error. Consequently, these results motivate the need for more advanced strategies, such as automated parameter optimization or adaptive nudging techniques, to dynamically determine the most effective μ value based on the local error evolution.

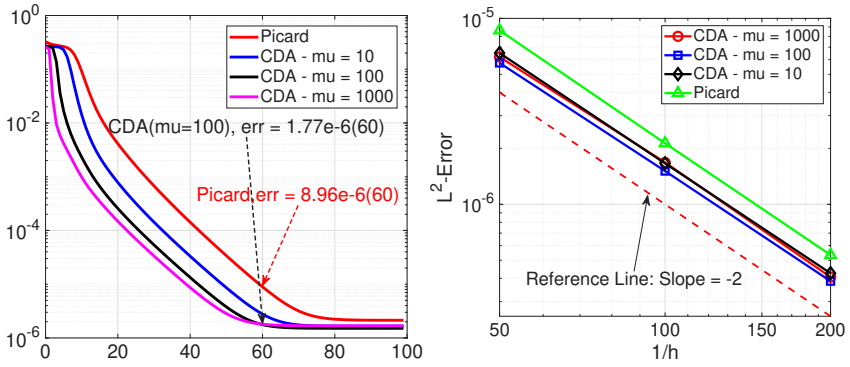

Fig. 3. Example 4.1: Influence of the nudging parameter μ on convergence history (left) and spatial convergence order (right) for $p = 1.1, s = 0.97$.

4.2 Example 4.2 - Less smooth solution

The exact solution and domain are chosen the same as previous test but here we denote $r = \sqrt{x^2 + y^2}$. If $\alpha = \frac{p-s}{p-1} < 1$, the gradient $\nabla u \approx r^{\alpha-1}$ blows up as $r \to 0$.

Case 2.1. CDA-Picard-Anderson Approach. As we observed in the previous test, when $p \to 3$, the required iteration counts are increasing significantly. In order to speed up the nonlinear solver, we will integrate the powerful Anderson acceleration scheme. Let $h = 0.02, H = 0.2, p = 3.0, s = 0.6, \mu = 100$, $m = 3$ with a stopping tolerance of 10^{-6}.

Fig. 4 illustrates the L^2 error (left) and the residual (right) convergence histories for four different schemes: standard Picard, Anderson Acceleration, CDA-enhanced Picard, and CDA-enhanced Anderson Acceleration.

– In this highly nonlinear and degenerate regime ($p = 3.0$), the standard Picard iteration (blue line) converges very slowly, taking nearly 10^3 iterations to

ICCS Camera Ready Version 2026
To cite this paper please use the final published version:
DOI: 10.1007/978-3-032-29918-5_11

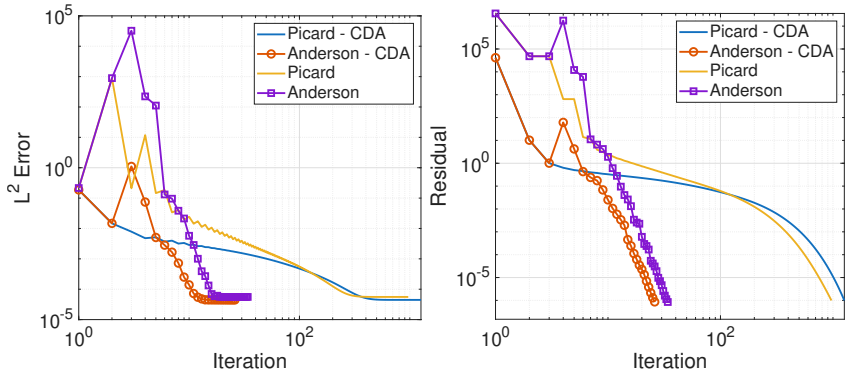

Fig. 4. Example 4.2: Convergence history of L^2 error (left) and residual (right) comparing standard, Anderson-accelerated, and CDA-enhanced solvers for $p = 3.0, s = 0.6$.

reach the tolerance. The introduction of Anderson Acceleration (purple line) significantly speeds up this process, reducing the iteration count by nearly an order of magnitude.

- Comparing the standard Picard (blue) with the CDA-enhanced Picard (yellow/green line), it is evident that the CDA term alone provides a strong "nudging" effect that forces a more rapid initial descent in both error and residual, though Anderson acceleration is still needed for the fastest final convergence.
- The CDA-enhanced Anderson method (orange line) demonstrates the most efficient performance. By combining the stabilization of the continuous data assimilation ($\mu = 100$) with the acceleration of the Anderson scheme ($m = 3$), the error and residual drop much faster than in any other algorithms.

Case 2.2 CDA-Picard-Anderson in Degenerate Case In this test, we consider a degenerate p-Laplace problem with $p = 3.5, s = 0.6, h = 0.02, \mu = 100, m = 3, H = 0.2$ with a maximum of 500 iterations. Fig. 5 illustrates the convergence behavior of the residual (right) and the L^2 error (left) for standard Picard, Anderson Acceleration ($m = 3$), and the combined CDA-enhanced Anderson Acceleration ($\mu = 100$).

- The standard Picard iteration (yellow line) exhibits extremely poor performance in this regime, characterized by a very shallow convergence slope that fails to reach the stopping criterion even after 500 iterations. While standard Anderson Acceleration (purple line) provides a significant speedup.
- The CDA-enhanced Anderson scheme (blue line) is clearly the most robust and efficient solver. By combining the spatial stabilization of Continuous Data Assimilation ($\mu = 100$) with the Anderson Acceleration ($m = 3$), this hybrid method achieves the fastest convergence.

ICCS Camera Ready Version 2026
To cite this paper please use the final published version:
DOI: 10.1007/978-3-032-29918-5_11

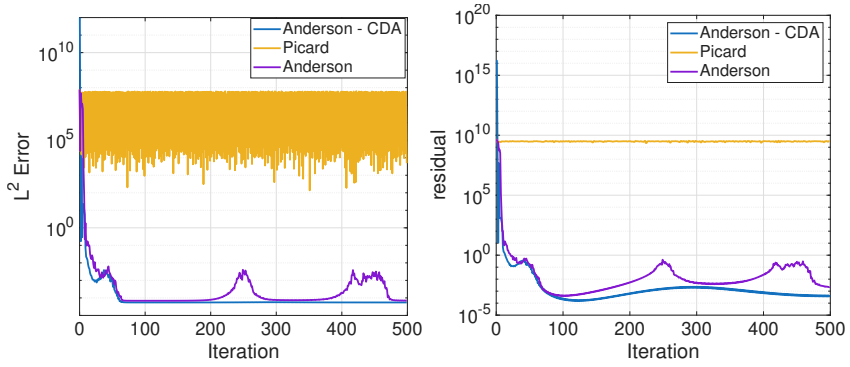

Fig. 5. Example 4.2: Comparison of L^2 error (left) and residual (right) convergence for standard Picard, Anderson Acceleration, and CDA-enhanced Anderson schemes at $p = 3.5, s = 0.6$.

– In the final stages of convergence, the standard Anderson acceleration (purple line) suffers from significant oscillatory behavior and residual spikes. These instabilities suggest that the Anderson optimization struggles with the high nonlinearity of the $p = 3.5$ case. In contrast, the CDA-enhanced Anderson scheme (blue line) exhibits a much smoother and more monotonic decay. This indicates that the CDA term acts as a critical spatial regularizer, guiding the solution and suppressing the instabilities encountered in degenerate regimes.

Case 2.3 Hybrid Picard-Newton Strategy As observed above, the residual decay becomes significantly slower as the residual values decrease. To further accelerate the nonlinear solver, we integrate a Newton iteration once the residual falls below a predefined switching tolerance, which we set here as $tol_{\text{switch}} = 10^{-3}$. Since the CDA-Picard-Anderson scheme provides a robust initial guess that lies within the convergence ball of second-order methods, we can reliably initiate the Newton solver using the same configuration established in Case 2.2.

Figure 6 illustrates the performance of the hybrid Picard-Newton strategy. The pre-solvers are chosen as the standard Anderson iterations (denoted as Anderson) and CDA-enhanced Picard-Anderson iterations (denoted as Anderson - CDA). Here we set $tol_{\text{switch}} = 10^{-3}$ and $\mu = 100, m = 3, h = 0.01, p = 3.5, s = 0.6, tol = 1e-12, H = 0.2$.

– The CDA-enhanced Anderson scheme (blue line) reaches the Newton switching tolerance ($tol_{\text{switch}} = 10^{-3}$) significantly faster than the standard Anderson method. Specifically, the CDA-enhanced version triggers the Newton solver at iteration 37, whereas the standard version requires 77 iterations to reach the same threshold.

ICCS Camera Ready Version 2026
To cite this paper please use the final published version:
DOI: 10.1007/978-3-032-29918-5_11

– Once the Newton iteration begins (indicated by the vertical dashed lines), both methods exhibit the rapid, quadratic convergence. However, the CDA-enhanced path reaches the final target tolerance of 10^{-12} in nearly half the total number of iterations compared to the non-enhanced version.
– The Anderson-CDA scheme not only significantly accelerates convergence but also achieves a lower final error floor compared to the standard Anderson method. This suggests that the continuous data assimilation provides a superior regularization effect that allows the solver to reach a more precise numerical solution in high-precision regimes.

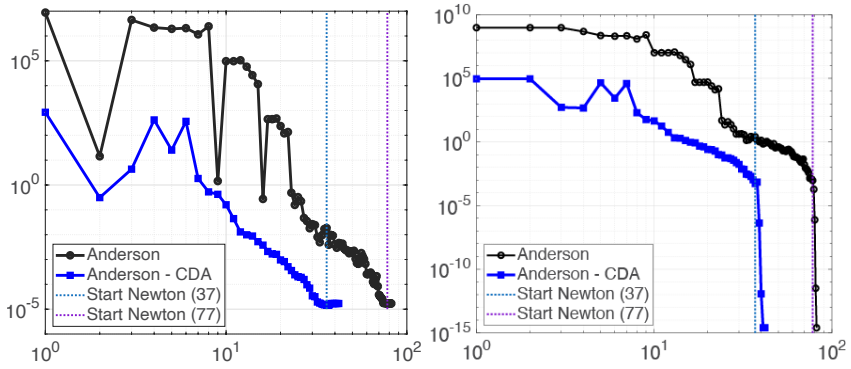

(a) L^2-error (b) Residual

Fig. 6. Example 4.2: erformance comparison of the hybrid Picard-Newton strategy using standard Anderson versus CDA-enhanced Anderson pre-solvers.

4.3 Example 4.3 - Unit Disk Domain

For a circular domain with radius $R = 1$, we investigate two distinct test cases to evaluate the robustness of our approach.

Case 3.1 - a degenerate solution (shear-thickening) Consider a case with $f = 10$ and $p = 4$, where the exact solution is given by,

$$u(r) = \frac{p-1}{p}\left(\frac{f}{2}\right)^{\frac{1}{p-1}}(1 - r^{\frac{p}{p-1}}).$$

The exact solution is plotted in Fig. 7 (left). Due to the strong nonlinearity inherent in this problem, standard Picard iterations fail to reach the switching tolerance tol_{switch}. To address this, we perform 4 initial Picard iterations to provide a suitable starting point, followed by Newton's method for the nonlinear solve. We compare the performance of the standard Newton method with the CDA-enhanced Newton scheme using $h = 0.02$ and $H = 0.2$ (Fig. 7 (center)).

ICCS Camera Ready Version 2026
To cite this paper please use the final published version:
DOI: 10.1007/978-3-032-29918-5_11

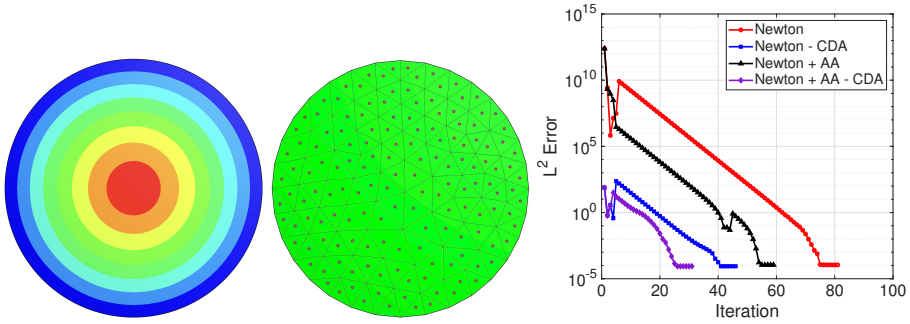

Fig. 7. Example 4.3: Plot of exact solution (left), coarse mesh observation (center), and L^2-error convergence (right).

Fig. 7 (right) illustrates the L^2-error convergence for the degenerate p Laplace problem ($p = 4$) on a unit disk. The plot compares four different solver configurations: standard Newton, Newton with CDA, Newton with AA, and a combined Newton-AA-CDA approach. The standard Newton method (red line) shows the slowest convergence, requiring approximately 83 iterations to reach the error floor. The introduction of Anderson Acceleration (Newton + AA, black line) significantly improves efficiency, reducing the iteration count to roughly 59. Both CDA-enhanced methods (blue and purple lines) demonstrate a much sharper initial descent in error. The Newton-CDA approach (blue line) reaches the error floor in approximately 48 iterations. The combined Newton + AA - CDA method (purple line) is the most efficient, achieving full convergence in just under 30 iterations. Furthermore, the CDA-Newton method improves the accuracy of the numerical solution, as the converged L^2-error decreases from 1.11×10^{-4} to 8.75×10^{-5}.

Case 3.2 - A Singular Solution (shear-thinning) Consider the highly shear-thinning case where $p = 1.5$. The exact solution is given by: $u(r) = r^{\frac{p-2}{p-1}}$. In this example, the exact solution exhibits a singularity at the origin. While achieving a reliable solution typically requires adaptive mesh refinement to increase resolution near the singularity, our primary objective is to evaluate the comparative performance of the CDA-Newton and standard Newton schemes. Consequently, all computations are performed on uniform grids with $h = 0.01$ and coarse observations on grid with size $H = 0.2$.

Fig. 8 illustrates the exact solution (left), the standard Newton solution (center), and the CDA-Newton solution (right). A critical observation is that while the standard Newton solver reaches a high-precision residual tolerance of 10^{-12} in fewer than 9 iterations, it completely fails to capture the underlying singularity. Instead, it converges to a non-physical global value of 1, effectively "missing" the essential physics at the center of the disk. By incorporating observed data

ICCS Camera Ready Version 2026
To cite this paper please use the final published version:
DOI: 10.1007/978-3-032-29918-5_11

on a coarse mesh ($H = 0.2$), the CDA-enhanced solver provides the necessary spatial regularization to overcome this numerical artifact. As shown in the rightmost panel, the hybrid scheme successfully captures the singular behavior and the accurate values near the origin—details that the standard scheme entirely overlooks despite its apparent convergence.

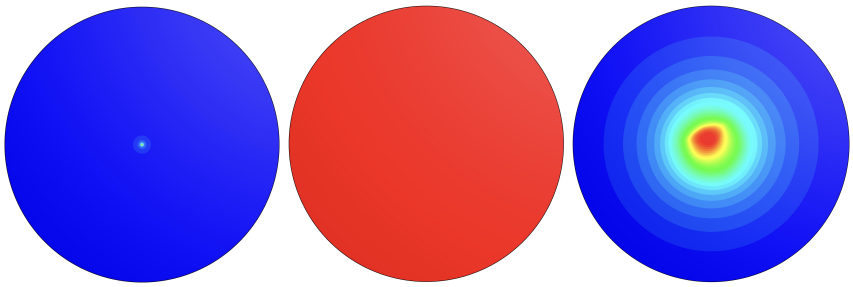

Fig. 8. Example 4.3: Comparison of exact, standard Newton, and CDA-Newton solutions for the singular shear-thinning problem ($p = 1.5$) on a unit disk.

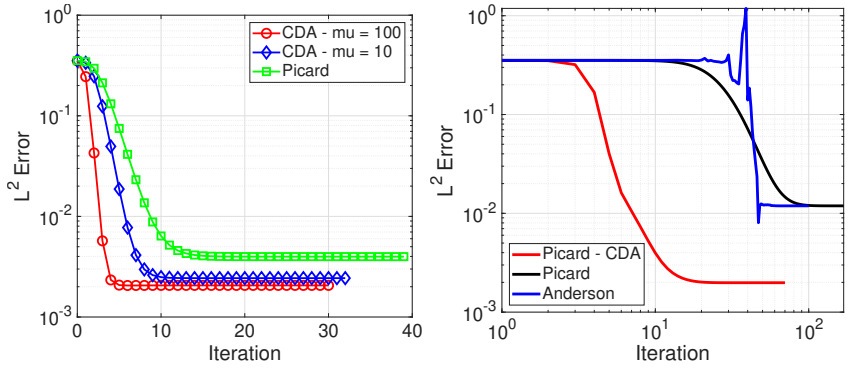

Fig. 9. Example 4.4: Convergence and Error Profiles

4.4 Example 4.4 - 3 Dimensional p-Laplace equation

For our three-dimensional evaluation, we consider the domain $\Omega = [0, 1]^3$ with a shear-thinning parameter $p = 1.5$. The exact solution is defined as $u = \sin(\pi x)\sin(\pi y)\sin(\pi z)$. Here we choose $H = 0.4, h = 0.04$.

ICCS Camera Ready Version 2026
To cite this paper please use the final published version:
DOI: 10.1007/978-3-032-29918-5_11

Fig. 9 illustrate the results of 3D p-Laplacian test ($p = 1.5$) comparing the standard Picard iteration with the CDA-enhanced and Anderson-accelerated versions. We observe:

- Fig. 9 (left) presents the L^2 error convergence for the CDA-enhanced Picard iteration ($\mu = 100, \mu = 10$) and Picard iteration. The convergence rate is sensitive to the strength of the data assimilation term. The standard Picard iteration (green square line) exhibits the slowest convergence, reaching an error floor of approximately 5×10^{-3} after 40 iterations. In contrast, increasing μ accelerates the initial error reduction. With $\mu = 100$ (red circle line), the solver achieves the target error level in fewer than 10 iterations, demonstrating a sharp initial descent. This indicates that the coarse-mesh observations ($H = 0.4$) provide sufficient global information to "nudge" the solution rapidly toward the correct state, even when the observation grid is ten times coarser than the simulation grid.
- In Fig. 9 (right), the comparison of L^2 error convergence for the 3D p-Laplace equation ($p = 1.5$) reveals that the Picard-CDA hybrid scheme significantly outperforms both standard Picard and standalone Anderson acceleration. While the standard Picard iteration converges slowly toward an error floor of 5×10^{-3}, the integration of Continuous Data Assimilation (CDA) provides essential spatial regularization that flattens the error profile much earlier, reaching the target precision in fewer than 10 iterations. This synergistic effect, further enhanced by Anderson acceleration, demonstrates that leveraging even coarse-mesh observations can reduce the required iteration count by over 75%, effectively stabilizing the solver in high-dimensional singular regimes while drastically lowering computational overhead.

5 Conclusion

This study introduced a hybrid framework for the p-Laplace equation by integrating CDA, AA, and Newton's Method. Our results demonstrate that this multi-stage strategy effectively overcomes convergence difficulties in both singular ($p < 2$) and degenerate ($p > 2$) regimes. Benchmarks in 2D and 3D reveal that CDA acts as a powerful spatial regularizer, suppressing oscillations and guiding the solver toward physical solutions. The AA-Newton transition provides synergistic global stability and local quadratic convergence, achieving high-precision results with significantly fewer iterations than standard Picard schemes.

Future work will focus on developing adaptive nudging schemes and evaluating the framework's robustness against noisy observations, reflecting more realistic data scenarios.

Acknowledgments. The work of L. Mu is partially supported by the National Science Foundation under the grant DMS-2309557.

ICCS Camera Ready Version 2026
To cite this paper please use the final published version:
DOI: 10.1007/978-3-032-29918-5_11

References

1. Azouani, A., Olson, E., Titi, E.S.: Continuous data assimilation using general interpolant observables. Journal of Nonlinear Science **24**(2), 277–304 (2014)
2. Barrett, J.W., Liu, W.B.: Finite element approximation of the p-laplacian. Math. Comput. **61**(204), 523–537 (1993)
3. Dallas, M., Pollock, S., Rebholz, L.G.: Analysis of an adaptive safeguarded Newton-Anderson algorithm of depth one with applications to fluid problems. arXiv preprint arXiv:2402.09295 (2024)
4. Diegel, A.E., Rebholz, L.G.: Continuous data assimilation and long-time accuracy in a C^0 interior penalty method for the Cahn–Hilliard equation. Applied Mathematics and Computation **424**, 127042 (2022)
5. Diening, L., Kreuzer, C.: Linear convergence of an adaptive finite element method for the p-laplacian equation. SIAM Journal on Numerical Analysis **46**(2), 614–638 (2008)
6. Evans, C., Pollock, S., Rebholz, L.G., Xiao, M.: A proof that Anderson acceleration improves the convergence rate in linearly converging fixed-point methods. SIAM Journal on Numerical Analysis **58**(1), 788–810 (2020)
7. Farhat, A., Lunasin, E., Titi, E.S.: On the Charney conjecture of data assimilation employing temperature measurements alone. Mathematics of Climate and Weather Forecasting **2**(1), 61–74 (2016)
8. Ferreira, R., De Pablo, A.: Numerical blow-up for the p-laplacian equation with a source. Comput. Methods Appl. Math. **5**(2), 137–154 (2005)
9. García-Archilla, B., Li, X., Novo, J., Rebholz, L.G.: Enhancing nonlinear solvers for the Navier–Stokes equations with continuous (noisy) data assimilation. Computer Methods in Applied Mechanics and Engineering **424**, 116903 (2024)
10. Haggar, M.D., Mbehou, M., Njifenjou, A.: Crank-Nicolson finite element methods for nonlocal problems with p-laplace-type operator. J. Math. Comput. Sci. **33**, 57–70 (2024)
11. Huang, Y.Q., Li, R., Liu, W.: Preconditioned descent algorithms for p-laplacian. J. Sci. Comput. **32**, 343–371 (2007)
12. Kim, K.Y.: Error estimates for a mixed finite volume method for the p-laplacian problem. Numer. Math. **101**(1), 121–142 (2005)
13. Di Leoni, P.C., Mazzino, A., Biferale, L.: Synchronization to big data: nudging the Navier–Stokes equations for data assimilation of turbulent flows. Physical Review X **10**(1), 011023 (2020)
14. Li, X., Hawkins, E., Rebholz, L.G., Vargun, D.: Accelerating and enabling convergence of nonlinear solvers for Navier–Stokes equations by continuous data assimilation. Computer Methods in Applied Mechanics and Engineering **416**, 116361 (2023)
15. Luo, Z., Teng, F.: An effective finite element newton method for 2D p-laplace equation with particular initial iterative function. J. Inequalit. Appl. **2016**, 1–24 (2016)
16. Pollock, S., Zhu, Y.: Uniqueness of discrete solutions of nonmonotone PDEs without a globally fine mesh condition. Numerische Mathematik **139**(4), 845–865 (2018)

ICCS Camera Ready Version 2026
To cite this paper please use the final published version:
DOI: 10.1007/978-3-032-29918-5_11